

# Edge-orientation processing in first-order tactile neurons

J Andrew Pruszynski & Roland S Johansson

**A fundamental feature of first-order neurons in the tactile system is that their distal axon branches in the skin and forms many transduction sites, yielding complex receptive fields with many highly sensitive zones. We found that this arrangement constitutes a peripheral neural mechanism that allows individual neurons to signal geometric features of touched objects. Specifically, we observed that two types of first-order tactile neurons that densely innervate the glabrous skin of the human fingertips signaled edge orientation via both the intensity and the temporal structure of their responses. Moreover, we found that the spatial layout of a neuron's highly sensitive zones predicted its sensitivity to particular edge orientations. We submit that peripheral neurons in the touch-processing pathway, as with peripheral neurons in the visual-processing pathway, perform feature extraction computations that are typically attributed to neurons in the cerebral cortex.**

Visual and tactile sensory processing both involve neural mechanisms that extract high-level geometric features of a stimulus, such as the orientation of an edge, by integrating information from many low-level inputs<sup>1–5</sup>. Although geometric feature extraction is generally attributed to neural processing in the cerebral cortex<sup>6,7</sup>, there is growing evidence in the visual system that feature extraction begins very early in the processing pathway<sup>8</sup>, even at the level of first-order (that is, bipolar) neurons in the retina<sup>9</sup>. We found that feature extraction also begins very early in the tactile processing pathway, at the distal arborization of first-order tactile neurons.

First-order neurons in the tactile system have distal axons that branch in the skin and form many transduction sites, yielding complex receptive fields with many highly sensitive zones<sup>10–18</sup>. The functional consequences of this spatial arrangement are unknown. Our general hypothesis is that this arrangement constitutes a peripheral neural mechanism for signaling geometric features of touched objects. We specifically tested whether first-order tactile neurons signal information about a canonical geometric feature, namely edge orientation<sup>4</sup>, and whether such edge orientation sensitivity relates to the spatial layout of a neuron's transduction sites. We focused on first-order tactile neurons innervating Meissner (fast-adapting type 1, FA-1) and Merkel (slow-adapting type 1, SA-1) end organs in the human fingertips<sup>19</sup> because they branch in the skin, have receptive fields with many highly sensitive zones<sup>17,18</sup> and are critical for conveying detailed spatial information about touched objects<sup>20</sup>.

Previous observations that a neuron's highly sensitive zones are non-uniformly distributed within its receptive field<sup>17,18</sup> motivated two key predictions. First, we predicted that the intensity of a neuron's response would signal edge orientation because its firing rate would increase with the degree of spatial coincidence between the neuron's highly sensitive zones and local tissue deformations caused by an edge moving across the skin<sup>13,18</sup>. That is, for a given neuron, some edge orientations show more spatial coincidence than others, and therefore yield stronger responses. Second, we predicted that the temporal structure of a neuron's response would signal the orientation of an

edge moving across its receptive field. That is, the temporal structure of the evoked action potentials is defined by the sequential stimulation of the neuron's highly sensitive zones, which in turn depends on edge orientation. Our results confirmed both of these predictions.

## RESULTS

We recorded action potentials from 26 FA-1 and 21 SA-1 neurons innervating the human fingertips. Isolated neurons were stimulated by repeatedly scanning tactile stimuli across their receptive field<sup>21</sup> at a speed (30 mm s<sup>-1</sup>) and contact force (0.4 N) typical for haptic exploration<sup>22</sup>. A subset of neurons (7 FA-1 and 7 SA-1) was stimulated at three additional speeds (32.5, 42.4 and 78.4 mm s<sup>-1</sup>). The stimulus pattern, wrapped around a rotating drum, consisted of various raised shapes, including lines with different orientations and three small dots used for generating a sensitivity map of the receptive field (**Fig. 1a** and **Supplementary Fig. 1**). The drum was advanced axially during the revolutions to incrementally pass the whole pattern across the receptive field, yielding a spatial event plot in which each tick mark represents the occurrence of an action potential plotted with respect to the position of the drum when it occurred<sup>21</sup>. Consistent with previous studies on analogous neurons in monkeys<sup>23</sup>, both FA-1 and SA-1 neurons produced a broadly isomorphic representation of the stimulus pattern, such that the spatial event plot resembled the relief of the stimulus pattern (**Fig. 1a**).

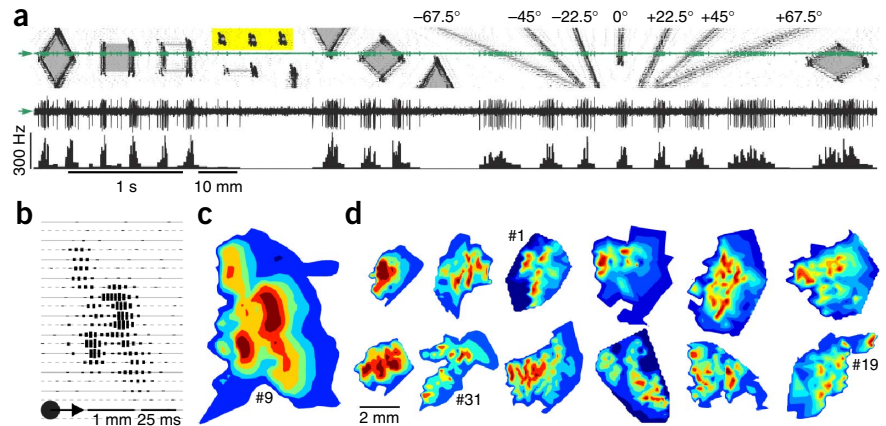
The core tenet of our hypothesis is that a neuron's response to particular edge orientations relates to the spatial arrangement of its multiple transduction sites. We estimated the spatial layout of a neuron's transduction sites by generating a sensitivity map of its receptive field based on its instantaneous firing rate in response to the small dot stimuli as a function of drum position (**Fig. 1b,c**). As in previous studies using both scanning<sup>18</sup> and punctate stimuli<sup>17</sup>, our neurons exhibited multiple non-uniformly distributed zones of high sensitivity (**Fig. 1d**) and most had elliptical, rather than circular, receptive fields (FA-1, 73%; SA-1, 81%;  $\chi^2$  test of variance,  $P < 0.05$ , corrected for 47 comparisons; median eccentricity = 1.9 and 1.8, respectively).

Physiology Section, Department of Integrative Medical Biology, Umeå University, Umeå, Sweden. Correspondence should be addressed to J.A.P. ([andrew.pruszynski@gmail.com](mailto:andrew.pruszynski@gmail.com)).

Received 27 June; accepted 8 August; published online 31 August 2014; doi:10.1038/nn.3804

**Figure 1** Stimuli and sensitivity maps.

(a) Top, spatial event plot from an exemplar neuron (SA-1: #9) where tick marks represent action potentials and whose height is proportional to the instantaneous firing rate<sup>18</sup>. Raised portions of the scanned stimulating surface are shown in gray. Yellow area indicates the small dot stimuli used to map receptive fields. Labels indicate the orientation of the lines used for detailed analysis. The 0° line stimulus is perpendicular to the rotation direction of the drum. Pairs of positive and negative line angles (that is,  $\pm 22.5^\circ$ ,  $\pm 45^\circ$ ,  $\pm 67.5^\circ$ ) indicate complementary edge orientations. Middle and bottom, raw neural signal and calculated instantaneous firing rate from a single rotation of the stimulating drum. (b) Close-up of the spatial event plot in a focusing on the small dot stimuli. (c) Receptive field in b represented as a sensitivity map in which brighter colors indicate higher instantaneous firing rates. (d) Sensitivity maps from 12 neurons, each normalized to their own peak firing rate for the small dot stimuli (top, FA-1; bottom, SA-1).



Consistent with our predictions, a neuron's response to an edge moving across its receptive field was often markedly multi-phasic and shaped by how an edge sequentially stimulated its highly sensitive zones (Fig. 2). Accordingly, the structure of a neuron's response appeared markedly affected by the orientation of the stimulating edge (Fig. 2d and Supplementary Fig. 2a,b). We formally investigated the link between the spatial layout of a neuron's highly sensitive zones and the structure of its responses by constructing a model that convolved each neuron's sensitivity map with the stimulus pattern. In essence, our model assumed that a neuron's instantaneous firing rate reflects the linear superposition of the stimulus and the spatial layout of the neuron's multiple transduction sites, as estimated from its sensitivity map. The model was markedly effective at predicting the observed responses (Fig. 2a,c,d). Correlating the predicted and observed firing-rate profiles for the seven line stimuli at the 30-mm s<sup>-1</sup> drum speed ( $n = 47$  neurons) revealed that the model accounted for 83.1% of the observed variance (Fig. 2e). There was no significant difference in model fit for FA-1 (mean  $R^2 = 82.3\%$ ) and SA-1 (84.0%) neurons (two-sample two-tailed  $t$  test,  $t_{45} = 0.62$ ,  $P = 0.5$ ), nor was there a significant

difference in model fit as a function of drum speed ( $n = 14$  neurons; mean  $R^2 = 83.7$ , 82.1, 82.2 and 82.0% at 30, 32.5, 42.4 and 78.4 mm s<sup>-1</sup>; one-way repeated-measures ANOVA,  $F_{3,36} = 1.3$ ,  $P = 0.3$ ).

Additional analyses confirmed that the model fit related to the detailed internal topography of a neuron's receptive field (Fig. 2e). First, rotating the empirically determined receptive field by 180°, such that its overall shape and orientation was identical, but the topography of the highly sensitive zones relative to the stimuli was highly disturbed, markedly reduced the quality of the predictions (one-sample two-tailed  $t$  test,  $t_{46} = 13.3$ ,  $P < 10^{-6}$ ). Second, randomly reassigning a neuron's responses to model predictions using another neuron's sensitivity map significantly reduced the quality of the fit (95% confidence interval (c.i.) of  $R^2 = 0.50 - 0.56$ ). Finally, alternative sensitivity maps with simpler internal topography all significantly reduced the quality of the predictions (all  $t_{46} > 13$ ,  $P < 10^{-6}$ ).

### Orientation signaling via intensity and temporal codes

Motivated by the outcome of the model, we explicitly tested our two predictions that first-order tactile neurons signal edge orientation via

**Figure 2** Observed and predicted neural responses. (a) Responses to a line stimulus (black bar) moving across a neuron's receptive field (FA-1: #8). Black trace represents the average firing rate profile of 12 passes (gray traces) across the receptive field aligned to the rotational position of the stimulus. The green trace represents the output of the model. (b,c) Empirical and predicted spatial event plot for the neuron shown in a. (d) Firing rate profiles, model predictions and raster plots for four exemplar neurons (left, FA-1; right, SA-1) and three line orientations ( $-22.5^\circ$ ,  $0^\circ$ ,  $+22.5^\circ$ ). (e) Green bar shows the correlation between the model prediction and the observed data for all line stimuli averaged across neurons when using the empirically determined sensitivity maps (error bars represent 1 s.e.m.,  $n = 47$ ). White error bar indicates model performance when randomly assigning observed responses and model predictions using the empirically determined receptive fields (95% c.i. of bootstrap; Online Methods). Black bars show the correlation when using alternative sensitivity maps (Online Methods): rotated (Rot), Gaussian (Gau) circular (c), Gaussian elliptical (e), uniform (Uni) circle (c), uniform ellipse (e).

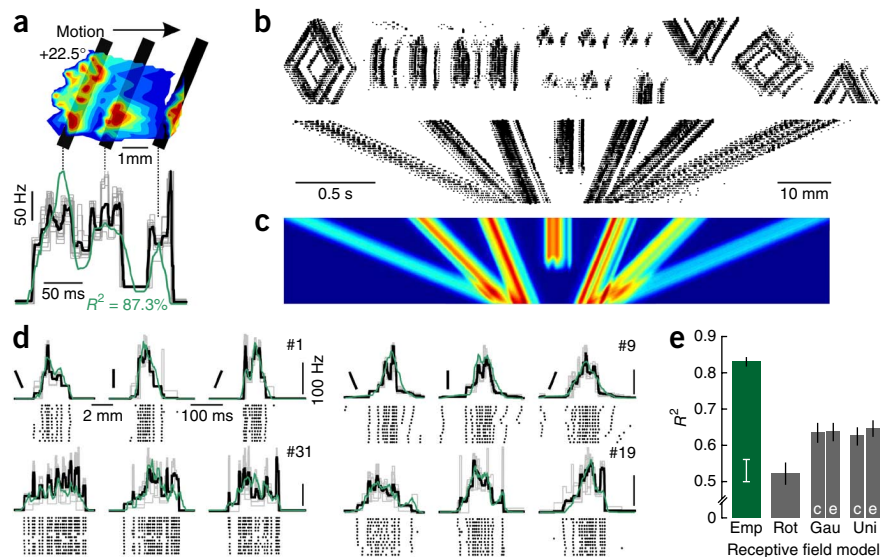
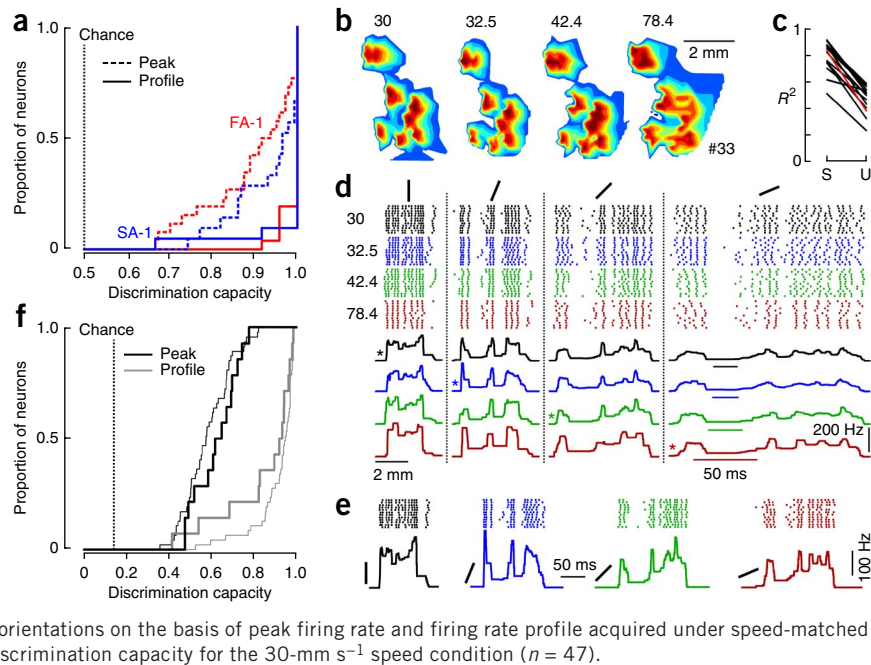


**Figure 3** Orientation discrimination and speed effect. **(a)** Cumulative distribution function representing the ability of an ideal observer to discriminate complementary line orientations on the basis of peak firing rates (dashed) and temporal profiles (solid) of FA-1 (red,  $n = 26$ ) and SA-1 (blue,  $n = 21$ ) neurons. The best discriminated line-orientation pair is shown. **(b)** Sensitivity maps for an exemplar SA-1 neuron at four different drum speeds. **(c)** Correlation between sensitivity maps for the same neurons across speed (S) and for the same speed across neurons (U). Lines indicate average correlations for single neurons ( $n = 14$ , red = neuron in **b**). **(d)** Raster plots and firing rate profile as a function of position for four line orientations and four speeds for the neuron shown in **b**. Asterisks indicate speed-matched data. **(e)** Raster plots and firing rate profiles as a function of time for four line orientations moving at the same effective speed (asterisks in **d**) for the neuron shown in **b**. **(f)** Cumulative distribution function representing discrimination capacity across all line orientations on the basis of peak firing rate and firing rate profile acquired under speed-matched conditions ( $n = 14$  neurons). Thin lines represent discrimination capacity for the  $30\text{-mm s}^{-1}$  speed condition ( $n = 47$ ).



both the intensity and temporal profile of their responses. To examine signaling by intensity, we compared peak firing rates evoked by line stimuli with complementary orientations relative to the motion of the stimulating surface (that is,  $\pm 22.5^\circ$ ,  $\pm 45^\circ$ ,  $\pm 67.5^\circ$ ) for each neuron collected at the  $30\text{-mm s}^{-1}$  drum speed. A targeted comparison between complementary edge orientations is critical because it factors out a neuron's potential sensitivity to the effective speed with which a stimulus moves across the skin<sup>18,21</sup>. Edge orientation routinely had a significant effect on the peak firing rates of both FA-1 and SA-1 neurons, averaging 38% and 34% of peak firing rate, respectively (two-sample two-tailed  $t$  test,  $n = 24$  repeated instances of edge stimuli (2 orientations, 12 repeats per orientation),  $P < 0.05$ , corrected for 141 comparisons; **Supplementary Fig. 2a–c**). We also applied receiver-operating characteristic (ROC) analysis to assess how well an ideal observer could discriminate complementary edges based on a neuron's peak firing rate. Both FA-1 and SA-1 neurons readily discriminated complementary edge orientations (**Fig. 3a** and **Supplementary Fig. 2d–f**). Notably, we found that those edge orientation pairs that were most difficult to discriminate according to the ROC analysis had more similar predicted peak firing rates according to our model than those pairs that were easiest to discriminate (one-sample two-sided  $t$  test,  $t_{46} = 17.9$ ,  $P < 10^{-6}$ ).

Another way to match the effective speed with which a stimulus moves across the skin is by changing the drum speed as a function of edge orientation. To that end, we stimulated a subset of neurons ( $n = 14$ ) at four drum speeds chosen so that each of the seven line stimuli moved across the skin at an effective speed of  $30\text{ mm s}^{-1}$ . Despite their complexity, sensitivity maps were markedly robust across speeds (**Fig. 3b**). Cross-correlating sensitivity maps revealed a significantly higher degree of similarity for the same neuron across speeds ( $R^2 = 81\%$ ) than across neurons for the same speed ( $R^2 = 47\%$ , one-sample two-tailed  $t$  test,  $t_{13} = 10.3$ ,  $P < 10^{-6}$ ; **Fig. 3c**). Firing rate profiles were also notably similar, showing only a marginal effect of stimulation speed (**Fig. 3d**). Using the speed-matched subset of these data (**Fig. 3d,e**), we calculated how well an ideal observer could classify the seven line stimuli on the basis of peak firing rate. For each neuron, we assessed how often the peak firing rate for an individual spike train ( $n = 12$  per edge) was closest to the mean peak firing rate

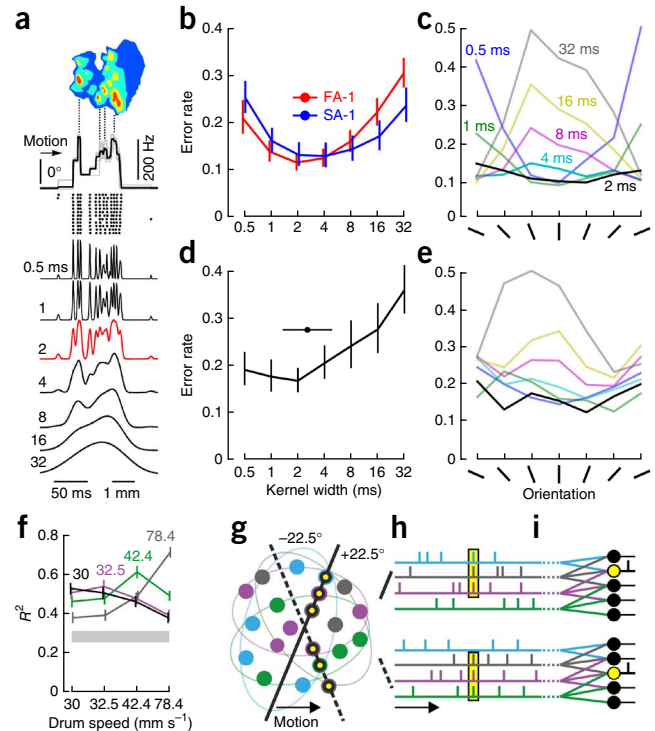
evoked by the same edge orientation as opposed to any of the other orientations. Consistent with the ROC analysis for complementary edge orientations, discrimination rates (mean and 95% c.i. = 61.2%, 53.9–68.0%) were much better than expected by chance ( $1/7 \approx 14\%$ ; **Fig. 3f**). Again, those edge orientations that were most difficult to discriminate had more similar predicted peak firing rates according to our model than those edges that were easiest to discriminate (one-sample two-sided  $t$  test,  $t_{13} = 8.8$ ,  $P < 10^{-6}$ ). Examining the assignment of incorrectly classified responses (that is, the confusion matrix) revealed a slight bias toward confusing complementary edges for more oblique edge orientations and nearest neighbors for more perpendicular edge orientations (**Supplementary Fig. 3a**).

To examine edge-orientation signaling by a neuron's temporal response profile, we calculated the probability of correctly discriminating edge orientation profiles for complementary edge orientations. For each neuron, we cross-correlated every pair of firing rate profiles for the  $30\text{-mm s}^{-1}$  drum speed, both within and across stimulating edges, and assessed how often the highest correlation for a particular spike train came from spike trains evoked by the same edge orientation as opposed to the complementary edge orientation. Notably, the spike trains of both FA-1 and SA-1 neurons were almost always correctly classified (mean and 95% c.i.: FA-1 = 91.7%, 87.2–93.2%; SA-1 = 91.6%, 88.8–93.8%; chance = 50%). Indeed, 85% of neurons showed perfect discrimination for at least one pair of complementary edges (**Fig. 3a**). Robust discrimination was also evident across all seven edge orientations for that subset of neurons collected under speed-matched conditions (mean and 95% c.i. = 90.6%, 82.2–95.2%, chance  $\approx 14\%$ ; **Fig. 3f**). Again, those edge orientations that were most difficult to discriminate according to the firing rate profile were more correlated according to the model than those edge orientations that were easiest to discriminate (one-sample two-sided  $t$  test: complementary edges,  $t_{46} = 15.3$ ,  $P < 10^{-6}$ ; speed matched,  $t_{13} = 7.0$ ,  $P < 10^{-5}$ ). We found no clear trend when examining the confusion matrix (**Supplementary Fig. 3b**).

#### Effect of precise timing of action potentials

Our analysis revealed that the temporal structure of a neuron's response provides substantial information about edge orientation.

**Figure 4** Timing of action potentials. (a) Top, sensitivity map, raster plot and firing rate profile for an exemplar neuron (FA-1: #32). Bottom, traces show probability density for the occurrence of action potentials as a function of time for various kernel widths. (b) Mean classification error rate ( $\pm 1$  s.e.m.) as a function of kernel-width averaged across line orientations and neurons for the 30-mm s<sup>-1</sup> drum speed. Horizontal bars indicate best kernel width (mean  $\pm 1$  s.d.) for FA-1 ( $n = 26$ ) and SA-1 ( $n = 21$ ) neurons. (c) Mean classification error rate as a function of edge orientation and kernel averaged across all 47 neurons for the 30-mm s<sup>-1</sup> drum speed. (d) Data are presented as in b for the speed-matched condition collapsed across neuron types ( $n = 14$ ). (e) Data are presented as in c under speed-matched conditions. (f) Each colored line represents the average correlation ( $\pm 1$  s.e.m.) between probability density profiles (2-ms kernel) for an edge orientation at that speed and the same edge orientation at the speed indicated on the horizontal axis. The gray area represents the 95% c.i. of correlations for a given edge orientation and all other edge orientations at each of the four speeds. (g) Four toy neurons (colors) with overlapping receptive and many highly sensitive zones (true overlap in fingertips: FA-1  $\approx 20$ , SA-1  $\approx 16$ ). Lines indicate two differently oriented stimuli. (h) For each neuron in g, a moving edge will sequentially stimulate highly sensitive zones and edge orientation will affect the sequence of evoked action potentials because different neurons have different distributions of highly sensitive zones. At a given instance, one edge will simultaneously stimulate one set of neurons and the other edge will simultaneously stimulate another set of neurons (yellow dots in g and yellow rectangle in h). (i) Each edge will cause temporally coincident inputs at different sets of higher order (for example, cuneate) neurons.



However, it does not establish the degree to which such information relies on precise timing of the action potentials, a factor known to be important for the processing of sensory information<sup>24–26</sup>. We examined this issue by imposing various amounts of noise on the timing of the recorded action potentials and quantifying how this noise affected a neuron's classification rate<sup>27,28</sup>. For each neuron, we convolved each spike train ( $n = 12$  per edge) with Gaussian kernels of various widths (0.5, 1, 2, 4, 8, 16 and 32 ms) that increasingly attenuated the temporal structure of the response (Fig. 4a). For each kernel, we then correlated every pair of convolved spike trains, both within and across stimulating edges<sup>28,29</sup>, and assessed how often the highest average correlation for a particular spike train came from spike trains evoked by the same edge orientation (Supplementary Fig. 4).

Across the population of neurons and edge orientations at the 30-mm s<sup>-1</sup> drum speed, we found a significant effect of kernel width on classification error rate ( $F_{6,270} = 31.0$ ,  $P < 10^{-6}$ ; Fig. 4b). On average, the 2-ms kernel yielded the lowest classification error rate for both FA-1 and SA-1 neurons. We found no significant main effect of neuron type on the overall error rate ( $F_{1,45} = 0.01$ ,  $P = 0.91$ ). However, neuron type did interact with kernel width ( $F_{6,270} = 3.3$ ,  $P = 0.004$ ), suggesting that classification performance of FA-1 neurons benefited more from precise spike timing than that for SA-1 neurons. For both the FA-1 and SA-1 neurons, kernel width and edge orientation markedly interacted with the error rate ( $F_{36,1620} = 21.6$ ,  $P < 10^{-6}$ ; Fig. 4c). Notably, with the 2-ms kernel, edge classification was similarly robust for all edge orientations. Narrower kernels yielded the lowest error rates for edges most perpendicular to the scanning direction, whereas wider kernels yielded the lowest error rates for more oblique edges that scanned the receptive field with lower effective speed. Similar results were obtained for those neurons collected under speed-matched conditions. Again, kernel width had a significant effect on edge classification ( $F_{6,72} = 13.1$ ,  $P < 10^{-5}$ ), with the 2-ms kernel yielding the lowest average error rate (Fig. 4d). However, the narrower kernels did not show a substantial increase in error rate with more oblique edges (Fig. 4e), likely because they were moving at the same effective speed as the

perpendicular (0°) edge at the 30-mm s<sup>-1</sup> drum speed, leading to slightly more consistent responses (Supplementary Fig. 5).

Overall, the spatial structuring of action potentials was notably invariant as a function of drum speed (Supplementary Fig. 5), as would be expected if the structuring arose because of the spatial distribution of a neuron's highly sensitive zones in the skin. We quantified this similarity by correlating spike trains smoothed with the 2-ms kernel with all other spike trains both across speed and edge orientation and found substantially stronger correlations between line stimuli of the same orientation across speeds than for line stimuli with different orientations for the same speed (Fig. 4f).

## DISCUSSION

The central result of our study is our finding that human first-order tactile neurons robustly signaled edge orientation, a capability previously attributed to neurons in the somatosensory cortex<sup>1–3,30</sup>. Our results indicate that edge orientation discrimination arises because different edges cause different patterns of spatial and temporal coincidence between a neuron's many transduction sites and the moving stimulus. Although we focused on straight edges, this peripheral mechanism may also permit first-order human tactile neurons to signal information about higher order aspects of a touched object, such as the curvature of an edge<sup>2</sup> and its motion direction<sup>30–32</sup>.

Current models of discriminative touch do not consider the computational consequences of a neuron's branching and subsequent connection to multiple transduction sites. This is likely because such models are based on neurophysiological studies in monkeys, which have emphasized that most first-order tactile neurons have simple receptive fields with one central zone of maximal sensitivity and a smooth decrease in sensitivity in all directions<sup>21,33–36</sup>. We believe that models that incorporate receptive fields with multiple highly sensitive zones are critical for understanding human touch. For example, such receptive fields provide a straightforward explanation for the psychophysical phenomenon of tactile hyper-acuity, in which people demonstrate tactile resolutions substantially better than predicted by the

spacing between receptive field centers<sup>35,37</sup>. Although a neuron with multiple highly sensitive zones can still only signal that the stimulus is located somewhere in its receptive field, a population of such neurons with overlapping receptive fields provides higher resolution. That is, for a given density of neurons, the theoretical limit of tactile resolution is defined by the spacing between their interdigitating highly sensitive zones, which is an order of magnitude less than the spacing between their receptive field centers.

Our model assumes that a neuron's response reflects the linear superposition of the stimulus and the location of the neuron's highly sensitive zones. Such superposition could arise if receptor potentials, generated at the transduction sites, traveled electronically to a common spike generation site in the parent axon<sup>13,18</sup>. Despite its simplicity, our model did well at predicting the magnitude and timing of neural responses to the various edge stimuli, although it tended to underestimate the depth of firing rate modulations in a response. One possible reason for the imperfection is that the model did not account for the complicated mechanical properties of the skin<sup>35</sup>, which itself can yield complex effects analogous to surround inhibition<sup>38</sup>. Specifically, our model could not capture the fact that our edges and small dot stimuli likely generate different distributions of stresses and strains at the transducer sites<sup>23</sup>. Another possible explanation for the imperfection is complex nonlinear interactions in the neuron's terminal arborization<sup>13,34,39,40</sup>. In contrast with electrotonic conduction to a common spike generation site in the parent axon, action potentials may be initiated at more distal branch points that are shared by more than one transduction site or even at the terminals of the axonal branches. Under such circumstances, the signals may not combine linearly because of the absolute refractoriness of the spike initiation site, collisions between orthodromically and antidromically propagating action potentials, and the recovery cycle at the transduction site after antidromic invasion of an action potential. Notably, skin mechanics along with nonlinear processing in the terminal arborization might enable first-order tactile neurons to perform a host of complex computations, akin to those that occur via integration across neurons and dendritic trees in the CNS<sup>41</sup>.

We found that individual neurons signaled edge orientation via both the intensity and the temporal structure of their responses. An individual neuron often responded with higher peak firing rates for some edge orientations than others, likely because of a higher degree of spatial coincidence with its highly sensitive zones. Given that the spatial layout of highly sensitive zones differs across neurons with overlapping receptive fields, the population of neurons could provide robust information about edge orientation. That is, a given orientation would cause some neurons to fire more intensely than others, and another orientation would preferentially recruit a different set of neurons. Such intensity-based population codes can indeed signal information about various sensory inputs and motor outputs<sup>42,43</sup>, including tactile edge orientation in the monkey somatosensory cortex<sup>1,3,30,32</sup> and fingertip force direction in human first-order tactile neurons<sup>44</sup>.

An individual neuron also responded to different edge orientations with different sequences of precisely timed action potentials, likely because different edges yielded different temporal patterns of spatial coincidence with one or more of the neurons' highly sensitive zones. At the population level, the temporal coincidence of action potentials across neurons with overlapping receptive fields could signal information about edge orientation. That is, a given orientation would yield epochs of synchrony in one set of neurons and another orientation would yield epochs of synchrony in a different set (Fig. 4g–i). There is indeed increasing appreciation that population codes based on synchrony at fine timescales can carry rich information

about sensory stimuli in various modalities<sup>45,46</sup>, including touch<sup>19,47</sup>. Synchrony codes can be effectively decoded via coincidence detection mechanisms in which higher order neurons preferentially respond when receiving many synchronous inputs<sup>48</sup>. Notably, our estimated precision in the timing (~2 ms) lies in the window required for effective coincidence detection supported by heterosynaptic mechanisms in somatosensory pathways<sup>49</sup>. By virtue of substantial neural convergence and divergence in the ascending somatosensory pathways<sup>19</sup>, coincidence detection mechanisms can provide moment-by-moment information about edge orientation, location and extent while factoring out potential confounds such as scanning speed. Indeed, we found that the spatial structuring of action potentials was markedly invariant with changes in scanning speed (Supplementary Fig. 5). Given the invariance of spatial structuring, the coincidence detection mechanism provides a straightforward explanation for psychophysical findings that tactile spatial acuity is maintained over a wide range of scanning speeds<sup>22</sup>.

## METHODS

Methods and any associated references are available in the [online version of the paper](#).

*Note: Any Supplementary Information and Source Data files are available in the online version of the paper.*

## ACKNOWLEDGMENTS

We thank B. Edin and D. Wolpert for their helpful comments on previous versions of this manuscript. We thank A. Bäckström, C. Hjältén, E. Jarocka, P. Jenmalm, P. Utsi and G. Westling for their technical and logistical support. This work was funded by the Swedish Research Council Projects 08667 and 22209, as well as by the Strategic Research Program in Neuroscience at the Karolinska Institute. J.A.P. received a long-term fellowship from the Human Frontier Science Program.

## AUTHOR CONTRIBUTIONS

Both authors contributed extensively to the work presented in this paper.

## COMPETING FINANCIAL INTERESTS

The authors declare no competing financial interests.

Reprints and permissions information is available online at <http://www.nature.com/reprints/index.html>.

- Bensmaia, S.J., Denchev, P.V., Dammann, J.F., Craig, J.C. & Hsiao, S.S. The representation of stimulus orientation in the early stages of somatosensory processing. *J. Neurosci.* **28**, 776–786 (2008).
- Yau, J.M., Pasupathy, A., Fitzgerald, P.J., Hsiao, S.S. & Connor, C.E. Analogous intermediate shape coding in vision and touch. *Proc. Natl. Acad. Sci. USA* **106**, 16457–16462 (2009).
- Fitzgerald, P.J., Lane, J.W., Thakur, P.H. & Hsiao, S.S. Receptive field properties of the macaque second somatosensory cortex: representation of orientation on different finger pads. *J. Neurosci.* **26**, 6473–6484 (2006).
- Hubel, D.H. & Wiesel, T.N. Receptive fields and functional architecture of monkey striate cortex. *J. Physiol. (Lond.)* **195**, 215–243 (1968).
- Shapley, R., Hawken, M. & Ringach, D.L. Dynamics of orientation selectivity in the primary visual cortex and the importance of cortical inhibition. *Neuron* **38**, 689–699 (2003).
- Hsiao, S. Central mechanisms of tactile shape perception. *Curr. Opin. Neurobiol.* **18**, 418–424 (2008).
- Ferster, D. & Miller, K.D. Neural mechanisms of orientation selectivity in the visual cortex. *Annu. Rev. Neurosci.* **23**, 441–471 (2000).
- Gollisch, T. & Meister, M. Eye smarter than scientists believed: neural computations in circuits of the retina. *Neuron* **65**, 150–164 (2010).
- Venkataramani, S. & Taylor, W.R. Orientation selectivity in rabbit retinal ganglion cells is mediated by presynaptic inhibition. *J. Neurosci.* **30**, 15664–15676 (2010).
- Cauna, N. Nerve supply and nerve endings in Meissner's corpuscles. *Am. J. Anat.* **99**, 315–350 (1956).
- Loof, F.J. Response of cat cutaneous mechanoreceptors to punctate and grating stimuli. *J. Neurophysiol.* **56**, 208–220 (1986).
- Paré, M., Smith, A.M. & Rice, F.L. Distribution and terminal arborizations of cutaneous mechanoreceptors in the glabrous finger pads of the monkey. *J. Comp. Neurol.* **445**, 347–359 (2002).

13. Goldfinger, M.D. Random-sequence stimulation of the G1 hair afferent unit. *Somatosens. Mot. Res.* **7**, 19–45 (1990).
14. Brown, A.G. & Iggo, A. A quantitative study of cutaneous receptors and afferent fibres in the cat and rabbit. *J. Physiol. (Lond.)* **193**, 707–733 (1967).
15. Lesniak, D.R. *et al.* Computation identifies structural features that govern neuronal firing properties in slowly adapting touch receptors. *eLife (Cambridge)* **3**, e01488 (2014).
16. Vallbo, A.B., Olausson, H., Wessberg, J. & Kakuda, N. Receptive field characteristics of tactile units with myelinated afferents in hairy skin of human subjects. *J. Physiol. (Lond.)* **483**, 783–795 (1995).
17. Johansson, R.S. Tactile sensibility in the human hand: receptive field characteristics of mechanoreceptive units in the glabrous skin area. *J. Physiol. (Lond.)* **281**, 101–125 (1978).
18. Phillips, J.R., Johansson, R.S. & Johnson, K.O. Responses of human mechanoreceptive afferents to embossed dot arrays scanned across fingerpad skin. *J. Neurosci.* **12**, 827–839 (1992).
19. Johansson, R.S. & Flanagan, J.R. Coding and use of tactile signals from the fingertips in object manipulation tasks. *Nat. Rev. Neurosci.* **10**, 345–359 (2009).
20. Johnson, K.O. The roles and functions of cutaneous mechanoreceptors. *Curr. Opin. Neurobiol.* **11**, 455–461 (2001).
21. Johnson, K.O. & Lamb, G.D. Neural mechanisms of spatial tactile discrimination: neural patterns evoked by braille-like dot patterns in the monkey. *J. Physiol. (Lond.)* **310**, 117–144 (1981).
22. Vega-Bermudez, F., Johnson, K.O. & Hsiao, S.S. Human tactile pattern recognition: active versus passive touch, velocity effects and patterns of confusion. *J. Neurophysiol.* **65**, 531–546 (1991).
23. Blake, D.T., Johnson, K.O. & Hsiao, S.S. Monkey cutaneous SA1 and RA responses to raised and depressed scanned patterns: effects of width, height, orientation, and a raised surround. *J. Neurophysiol.* **78**, 2503–2517 (1997).
24. Panzeri, S., Petersen, R.S., Schultz, S.R., Lebedev, M. & Diamond, M.E. The role of spike timing in the coding of stimulus location in rat somatosensory cortex. *Neuron* **29**, 769–777 (2001).
25. Gollisch, T. & Meister, M. Rapid neural coding in the retina with relative spike latencies. *Science* **319**, 1108–1111 (2008).
26. Johansson, R.S. & Birznieks, I. First spikes in ensembles of human tactile afferents code complex spatial fingertip events. *Nat. Neurosci.* **7**, 170–177 (2004).
27. Vázquez, Y., Salinas, E. & Romo, R. Transformation of the neural code for tactile detection from thalamus to cortex. *Proc. Natl. Acad. Sci. USA* **110**, E2635–E2644 (2013).
28. Schreiber, S., Fellous, J.M., Whitmer, D., Tiesinga, P. & Sejnowski, T.J. A new correlation-based measure of spike timing reliability. *Neurocomputing* **52–54**, 925–931 (2003).
29. Fellous, J.M., Tiesinga, P.H., Thomas, P.J. & Sejnowski, T.J. Discovering spike patterns in neuronal responses. *J. Neurosci.* **24**, 2989–3001 (2004).
30. Hyvärinen, J. & Poranen, A. Movement-sensitive and direction and orientation-selective cutaneous receptive fields in the hand area of the post-central gyrus in monkeys. *J. Physiol. (Lond.)* **283**, 523–537 (1978).
31. Warren, S., Hamalainen, H.A. & Gardner, E.P. Objective classification of motion- and direction-sensitive neurons in primary somatosensory cortex of awake monkeys. *J. Neurophysiol.* **56**, 598–622 (1986).
32. Pei, Y.C., Hsiao, S.S., Craig, J.C. & Bensmaia, S.J. Neural mechanisms of tactile motion integration in somatosensory cortex. *Neuron* **69**, 536–547 (2011).
33. Khalsa, P.S., Friedman, R.M., Srinivasan, M.A. & Lamotte, R.H. Encoding of shape and orientation of objects indented into the monkey fingerpad by populations of slowly and rapidly adapting mechanoreceptors. *J. Neurophysiol.* **79**, 3238–3251 (1998).
34. Phillips, J.R. & Johnson, K.O. Tactile spatial resolution. III. A continuum mechanics model of skin predicting mechanoreceptor responses to bars, edges, and gratings. *J. Neurophysiol.* **46**, 1204–1225 (1981).
35. Goodwin, A.W. & Wheat, H.E. Sensory signals in neural populations underlying tactile perception and manipulation. *Annu. Rev. Neurosci.* **27**, 53–77 (2004).
36. Vega-Bermudez, F. & Johnson, K.O. SA1 and RA receptive fields, response variability, and population responses mapped with a probe array. *J. Neurophysiol.* **81**, 2701–2710 (1999).
37. Loomis, J.M. Tactile pattern perception. *Perception* **10**, 5–27 (1981).
38. Vega-Bermudez, F. & Johnson, K.O. Surround suppression in the responses of primate SA1 and RA mechanoreceptive afferents mapped with a probe array. *J. Neurophysiol.* **81**, 2711–2719 (1999).
39. Eagles, J.P. & Purple, R.L. Afferent fibers with multiple encoding sites. *Brain Res.* **77**, 187–193 (1974).
40. Lindblom, Y. & Tapper, D.N. Integration of impulse activity in a peripheral sensory unit. *Exp. Neurol.* **15**, 63–69 (1966).
41. Branco, T. & Häusser, M. The single dendritic branch as a fundamental functional unit in the nervous system. *Curr. Opin. Neurobiol.* **20**, 494–502 (2010).
42. Britten, K.H., Shadlen, M.N., Newsome, W.T. & Movshon, J.A. The analysis of visual motion: a comparison of neuronal and psychophysical performance. *J. Neurosci.* **12**, 4745–4765 (1992).
43. Georgopoulos, A.P., Schwartz, A.B. & Kettner, R.E. Neuronal population coding of movement direction. *Science* **233**, 1416–1419 (1986).
44. Birznieks, I., Jenmalm, P., Goodwin, A.W. & Johansson, R.S. Encoding of direction of fingertip forces by human tactile afferents. *J. Neurosci.* **21**, 8222–8237 (2001).
45. Stanley, G.B. Reading and writing the neural code. *Nat. Neurosci.* **16**, 259–263 (2013).
46. Gire, D.H. *et al.* Temporal processing in the olfactory system: can we see a smell? *Neuron* **78**, 416–432 (2013).
47. Panzeri, S., Brunel, N., Logothetis, N.K. & Kayser, C. Sensory neural codes using multiplexed temporal scales. *Trends Neurosci.* **33**, 111–120 (2010).
48. König, P., Engel, A.K. & Singer, W. Integrator or coincidence detector? The role of the cortical neuron revisited. *Trends Neurosci.* **19**, 130–137 (1996).
49. Usrey, W.M. The role of spike timing for thalamocortical processing. *Curr. Opin. Neurobiol.* **12**, 411–417 (2002).

## ONLINE METHODS

**Study participants and general procedure.** 26 females and 18 males (19–38 years of age) participated after providing written informed consent in accordance with the Declaration of Helsinki. The Umeå University ethics committee approved the study. The general experimental methodology, procedure and apparatus have been described previously<sup>18,44</sup>. Action potentials from single first-order tactile neurons terminating in the glabrous skin of the index, long or ring finger were recorded with tungsten electrodes<sup>50</sup> inserted into the right median nerve at the level of the upper arm or wrist. Isolated neurons were classified as FA-1, SA-1, fast-adapting type 2 and slow-adapting type 2, according to previously described criteria<sup>19</sup>.

**Stimulus.** An embossed pattern mounted on a rotating drum repeatedly stimulated each isolated neuron's (26 FA-1 and 21 SA-1) receptive field along the proximal-distal axis of the finger (**Fig. 1a** and **Supplementary Fig. 1**). The embossed pattern was produced via a standard photo-etching technique using a photosensitive nylon polymer (Toyobo EF 70 GB, Toyobo). All the elements were 0.5 mm high. Line widths were 0.5 mm at the top and 0.8 mm at the base. The embossed dots were essentially truncated cones with a 0.4-mm diameter flat top and a base diameter of 0.7 mm. All of the elements were spaced at least 8 mm apart to ensure minimal interactions between elements<sup>18</sup>. A custom-built robotic device controlled the rotation and translation of the drum as well as the contact force between the drum and the receptor-bearing fingertip. To stabilize the fingers, we glued the nails to plastic holders firmly attached to a table that also supported the right arm and the robot. The stimulus pattern, wrapped around the drum, was repeatedly scanned across the neuron's receptive field at a speed of 30 mm s<sup>-1</sup>. A subset of neurons (7 FA-1 and 7 SA-1) was stimulated at three additional speeds: 32.5, 42.4 and 78.4 mm s<sup>-1</sup>. The order of presentation of all speed conditions was randomized. These speeds were chosen so that we could acquire responses where each oriented line stimulus (that is, edge orientation) moved across the skin at an effective speed of 30 mm s<sup>-1</sup>. This 'speed-matched' data set combined responses for the 0° line stimulus (that is, perpendicular to the scanning direction) at a drum speed of 30 mm s<sup>-1</sup>, with the ±22.5° line stimuli at a drum speed of 32.5 mm s<sup>-1</sup> (= 30/cosine (22.5°)), the ±45° line stimuli at a drum speed of 42.4 mm s<sup>-1</sup> and the ±67.5° line stimuli at a drum speed of 78.4 mm s<sup>-1</sup> (**Fig. 3d** and **Supplementary Fig. 5**). The drum was advanced 0.4 mm per revolution along its axis of rotation, causing the whole pattern to incrementally pass across the receptive field<sup>21</sup>. The instantaneous rotational position of the drum was monitored via an optical shaft encoder (AC36, Hengstler GmbH), which provided position resolution of 3 μm in the scanning direction. The contact force, perpendicular to the skin, was servo-controlled such that it was equal to ~0.4 N for those parts of the drum with no embossed stimuli.

**Data analysis and statistics.** We analyzed where action potentials occurred relative to the various items on the drum. This relationship was visualized using a two-dimensional spatial event plot by laying out the impulse sequences evoked on successive rotations as parallel rows of ticks where each row corresponded to a single rotation of the drum<sup>21</sup> (**Fig. 1a**). The horizontal and vertical coordinates of each action potential were determined using the rotational and axial position of the drum, respectively. Sensitivity maps of each receptive field were based on responses to the small dot stimuli. The axial spatial resolution of the map was 0.2 mm, although the drum was advanced 0.4 mm in the axial direction per revolution because the small dots were offset axially by 0.2 mm. The third small dot provided independent verification that our sensitivity map estimate was reproducible (average  $R^2$  between sensitivity maps > 0.95). As a general measure of receptive field eccentricity, we applied principal components analysis to the two-dimensional spatial distribution of action potentials.

All analyses of how well a neuron's response signaled information about edge orientation were based on 12 consecutive responses evoked by each of the seven line stimuli. For paired comparisons of complementary edge orientations based on peak firing rate, we calculated the area under the ROC curve as a measure of discriminability. Complementary line stimuli (that is, ±22.5°, ±45°, ±67.5°) were defined relative to the scanning direction as these edge orientations moved with the same effective speed relative to the skin. For neurons collected under

speed-matched conditions, we used a different approach to make comparisons across all seven edge orientations. That is, we quantified how well the intensity of a neuron's response signaled edge orientation by calculating how frequently the peak firing rate evoked by each repetition of a particular line stimulus was closer to the average peak firing rate evoked by the same line stimulus than to any of the other six line stimuli. We also quantified how well a neuron's firing rate profile signaled edge orientation by calculating the probability of correctly classifying an observed profile to the edge orientation that evoked it. In this analysis, we cross-correlated every pair of firing rate profiles both within and across line stimuli. For each profile, we then averaged the correlations as a function of line stimulus and asked how often the highest average correlation resulted from the same line stimulus as opposed to either the complementary line stimulus (for comparisons at the standard 30-mm s<sup>-1</sup> drum speed) or to any of the other six line stimuli (for comparisons under speed-matched conditions).

To understand the degree to which correct classification based on the temporal structure of the response relied on the precise timing of action potentials, we used a correlation-based measure of spike timing reliability that provided an estimate of the similarity between pairs of individual spike trains<sup>28,29</sup>. After extracting spike times, we generated smoothed traces by convolving each of the extracted spike trains with a Gaussian function of fixed width<sup>27,28</sup>. This procedure replaced each spike by a standard waveform of known time span. We used seven Gaussian kernels of varying width (0.5, 1, 2, 4, 8, 16, 32 ms) and performed pairwise cross-correlations both in and across line stimuli. For each of these filtered representations, we then assessed how often the highest average correlation for a particular spike train came from spike trains evoked by the same edge orientation or by any of the other six edges. For a narrow kernel, spike timing can yield high reliability values only if the spike jitter is similar or smaller than the kernel width; a broad kernel decreases the influence of individual spike jitter (on a timescale below the kernel width) and the occurrence of additional and missing action potentials dominate the value of reliability<sup>27,28</sup>. The effect of orientation, kernel and neuron type on classification rate were assessed with a three-way mixed-design ANOVA, with orientation and kernel as within-group effects and neuron type as a between-group effect.

Data were Fisher or logit transformed when performing parametric statistics on correlation coefficients and proportions, respectively. In all cases, we defined a statistically significant outcome if  $P < 0.05$ . Where indicated, statistical tests were corrected for multiple comparisons using the Holm-Bonferroni method.

**Model of neural responses.** We constructed a simple quantitative model, with no free parameters, that predicted a neuron's time-varying response by convolving its empirically determined sensitivity map with the stimulus pattern. As such, the model assumed that a neuron's instantaneous firing rate reflected the linear superposition of the sensitivity map and the stimulus pattern. We quantified model performance by cross-correlating the predicted firing rate profiles and the average observed firing rate profiles for all seven line stimuli. We performed several control analyses using predictions based on different representations of each neuron's sensitivity map. This included (1) a circular receptive field matched for area with maximal sensitivity at its center and dropping off with a Gaussian profile<sup>35</sup>, (2) an elliptical receptive field matched for area and orientation (from the principal components analysis) with maximal sensitivity at its center and dropping off with a Gaussian profile<sup>35</sup>, (3) a circular receptive field matched for area with uniform sensitivity, (4) an elliptical receptive field matched for area and orientation with uniform sensitivity<sup>17</sup>, and (5) the empirically determined receptive field rotated by 180° relative to the direction of movement. We performed a bootstrap analysis whereby we randomly assigned each neuron's response to the seven line stimuli to model predictions using any neuron's sensitivity map. We then calculated the average correlation between the predicted and observed responses. This procedure was repeated 10,000 times to estimate the correlations that the model would produce by chance given the observed sensitivity maps.

A **Supplementary Methods Checklist** is available.

50. Vallbo, A.B. & Hagbarth, K.E. Activity from skin mechanoreceptors recorded percutaneously in awake human subjects. *Exp. Neurol.* **21**, 270–289 (1968).